Journal of Theoretical and Applied Physics (JTAP), Vol.16, No. 1, 162203 (1-6), 2022
Received 21 October 2021; Accepted 9 March 2022; [http://dx.doi.org/10.30495/jtap.162203]

Investigation of the Poynting flux ratio in the helix traveling wave tube

Mona Mehranfar, Shahrooz Saviz*, Davoud Dorranian

Abstract
The study deals with amplification of a propagating slow wave interacting with an annular hollow electron beam in a helix slow wave structure (SWS). The role of thermal plasma density in a ratio of the axial pointing flux in the plasma region is also investigated. This ratio is small for lower plasma densities. The effects of the variations of the hollow electron beam velocity on the normalized growth rate and the poynting flux ratio at the hybrid mode frequency are presented. The maximum gain is obtained in the frequency of hybrid mode and the poynting flux ratio reaches its maximum value at the hybrid mode frequency. Also is analyzed the trend of changes for the normalized growth rate for a different beam velocities. The results show that for all beam velocities the maximum growth rate is for hybrid mode frequencies. The numerical method used in this paper is complex transcendental.

Keywords
Hybrid mode, Slow wave structure.

Plasma Physics Research Centre, Science and Research Branch, Islamic Azad University, Tehran, Iran.
***Corresponding author**: shahrooz.saviz@srbiau.ac.ir

1. Introduction

Investigation into the helix traveling wave tube (TWT) started by Pierce four decades ago [1–3]. Initial works were based on a coupled-wave analysis while an electromagnetic analysis of Maxwell's equation was later introduced by Rydbeck [4] and Chu and Jackson [2]. Inserting plasma into the traveling wave tube to facilitate the electron beam performance has been studied by many authors [5]. Among them thermal plasma tecnology has also been investigated in increasing the gain of different systems [6].

In this paper, we investigated the effects of a thermal plasma injection into the helix TWT on the growth rate and the poynting flux ratio. For this purpose we developed a field theory by a solution of the fluid equation and Maxwell's equations. The growth rate of the modes is determined by the dispersion relation in the helix traveling wave tube. The dispersion relation is obtained by applying the appropriate boundary conditions at different regions. It has already been shown that the presence of thermal plasma enhances the growth rate of the system [7]. In recent years, the hybrid modes have received much attention from researchers. These modes are present in plasma loaded slow wave structure at frequencies where the phase velocities of the electromagnetic wave and slow plasma wave coincide.

The field of the hybrid mode was strong enough inside the plasma as well as near the structure, so the interaction of this mode with an electron beam inside the plasma caused the energy to be extracted from the beam as radiation. Poynting flux ratio in the helix traveling wave tube in the presence of the solid electron beam was investigated by Saturo Kobayashi and et al [8]. In this paper, we examined the same issue in the presence of the hollow electron beam.

2. The case of an annular electron beam

We used a hollow electron beam propagating through a plasma-loaded helix within the cylindrical drift tube. Our traveling wave tube consists of a helix that helps the propagation of an electromagnetic wave and an annular hollow electron beam which is produced by means of the electron gun on the left side of the tube. The thermal plasma is partially loaded inside the helix. The plasma is confined by a finite magnetic field $\mathbf{B}_0 = B_0\hat{e}_z$. The electrons of an electron beam influenced by the field of the wave will be bunched. So there will be an energy transfer from the electron beam to the wave and vice versa. The present manuscript is an improvement on the analysis in [7]. The circuit configuration in regions 1-5 in Fig. 1 consists of a conducting waveguide of radius R_w, a hollow electron beam with an inner radius of R_b and an outer radius of R_c, background thermal plasma of a radius R_p, and the helix of a radius R_h which is thin enough to be considered as a cylindrical sheath. For simplicity, we restrict the electron motion to the axial direction by applying a strong DC magnetic field parallel to the helix axis.

3. General formulation

The analysis of charge-electromagnetic wave interactions is simplified through Maxwell's equations. To calculate the fluctuating electric and magnetic fields in different regions,

first we start with the linear continuity and momentum transfer equations. We considered homogeneous plasma and the electrons are assumed to move in only one- dimension. We neglected the nonlinear effects. The equations are solved for small perturbations about a steady state as $n_e = n_{0e} + \delta n_e$, $v_e = v_{0e} + \delta v_e$ for electron beam and $n_p = n_{0p} + \delta n_p$, $v_p = \delta v_p$ for thermal plasma. These equations are as follows:
For electron beam:

$$[\frac{\partial}{\partial t} + v_{0e}\frac{\partial}{\partial z}]\delta n_e + n_{0e}\nabla.\delta v_e = 0 \quad (1)$$

$$[\frac{\partial}{\partial t} + v_{0e}\frac{\partial}{\partial z}]\delta v_e = \Omega_{ce}\hat{e}_z \times \delta v_e - (\frac{e}{\gamma_{0e} m_e})$$

$$[(I - \beta_{0e}^2 \hat{e}_z\hat{e}_z).\delta E + \beta_{0e}\hat{e}_z \times \delta B] \quad (2)$$

Here $\beta_{0e} = v_{0e}/c$ is the normalized axial velocity of the electron beam, $\gamma_{0e} = (1-\beta_{0e}^2)^{-0.5}$ is the relativistic factor, $\Omega_{ce} = eB_0/\gamma_{0e} m_e c$ is the electron cyclotron frequency and I is the unit dyadic. To calculate the perturbed quantities, we use the Fourier analysis representation as $\delta f(x,t) = \delta\hat{f}(r)\exp[ikz - i\omega t]$, where, k and ω represent the wave number and the angular frequency.
For thermal plasma:

$$\frac{\partial \delta n_p}{\partial t} + n_{0p}\nabla.\delta v_p = 0 \quad (3)$$

$$\frac{\partial \delta v_p}{\partial t} = -\frac{e}{m_e}\delta E + \gamma_{0e}\Omega_{ce}\hat{e}_z\delta v_p + \frac{\nabla P}{m_e n_{0p}} \quad (4)$$

We can derive the perturbed current density with the aid of 1 to 4 as follows. In region 2 we have:

$$\delta\hat{J}_I = \frac{i\omega_b^2}{4\pi\Delta\omega_0}[\frac{\omega}{\Delta\omega_0\gamma_{0e}^2}(\hat{e}_z.\delta\hat{E})\hat{e}_z$$
$$+\frac{i\Omega_{ce}\Delta\omega_0}{(\Delta\omega_0^2 - \Omega_{ce}^2)}(\hat{e}_z \times \delta\hat{E}_\perp - \beta_{0e}\delta\hat{B}_\perp)$$
$$+\frac{\Delta\omega_0^2}{(\Delta\omega_0 - \Omega_{ce}^2)}(\delta\hat{E}_\perp + \beta_{0e}\hat{e}_z \times \delta\hat{B}_\perp)$$
$$-\frac{iv_{0e}\Delta\omega_0}{(\Delta\omega_0 - \Omega_{ce}^2)}[\hat{e}_z\nabla_\perp.\delta\hat{E}_\perp - \beta_{0e}\nabla_\perp \times \delta\hat{B}_\perp]$$
$$-\frac{v_{0e}\Omega_{ce}}{(\Delta\omega_0^2 - \Omega_{ce}^2)}\hat{e}_z \times [\hat{e}_z(\hat{e}_z.\nabla_\perp \times \delta\hat{E}_\perp) + \beta_{0e}\hat{e}_z\hat{e}_z\nabla_\perp.\delta\hat{B}_\perp]$$
$$+\frac{i\omega_p^2\gamma_{0e}}{4\pi\omega}(\hat{e}_z.\delta\hat{E}) + \frac{\omega_T^2}{k\omega A}\frac{i\omega_p^2\gamma_{0e}k}{4\pi\omega^2}(\hat{e}_z.\delta\hat{E})$$
$$+\frac{i\omega_p^2\gamma_{0e}}{4\pi\omega}[\frac{-i\Omega_{ce}\gamma_{0e}}{\omega^2 - (\Omega_{ce}\gamma_{0e})^2}(\hat{e}_z.\nabla_\perp \times \delta\hat{E}_\perp)$$
$$+\frac{\omega}{\omega^2 - (\Omega_{ce}\gamma_{0e})^2}\nabla_\perp.\delta\hat{E}_\perp\hat{e}_z \quad (5)$$

where $\omega_b^2 = 4\pi n_{0e}e^2/\gamma_{0e}m_e$, $\omega_p^2 = 4\pi n_{0p}e^2/\gamma_{0e}m_e$, $\Delta\omega_0 = \omega - kv_0$, $\omega_T^2 = 3k_bT_ek^2/m_e$, and $A = 1 - \omega_T^2/\omega^2$.
In regions 1 and 3:

$$\delta\hat{J}_{II} = \frac{i\omega_p^2\gamma_{0e}}{4\pi\omega}(\delta\hat{E}_z + \frac{\omega_T^2}{k\omega A}(\frac{i\omega_p^2\gamma_{0e}k}{4\pi\omega^2}\delta\hat{E}_z$$
$$+\frac{\omega_p^2\gamma_{0e}}{4\pi\omega}[\frac{-i\Omega_{ce}\gamma_{0e}}{\omega^2 - (\Omega_{ce}\gamma_{0e})^2}(\hat{e}_z.\nabla_\perp \times \delta\hat{E}_\perp)$$
$$+\frac{\omega}{\omega^2 - (\Omega_{ce}\gamma_{0e})^2}\nabla_\perp\delta\hat{E}_\perp]))\hat{e}_z$$
$$+\frac{-i\Omega_{ce}\gamma_{0e}\omega}{\omega^2 - (\Omega_{ce}\gamma_{0e})^2}(\hat{e}_z \times \delta\hat{E}_\perp) + \frac{\omega^2}{\omega^2 - (\Omega_{ce}\gamma_{0e})^2}\delta\hat{E}_\perp \quad (6)$$

Similarly, the perturbed charge densities can be written as:

$$\delta\hat{\rho}_e = \frac{i\omega_b^2}{4\pi\Delta\omega_0^2}\frac{k}{\gamma_{0e}^2}(\hat{e}_z.\delta\hat{E})$$
$$-(\frac{i\Delta\omega_0^2}{\Delta\omega_0^2 - \Omega_{ce}^2})[\nabla_\perp.\delta\hat{E}_\perp - \beta_{0e}\hat{e}_z.\nabla_\perp \times \delta\hat{B}_\perp]$$
$$-(\frac{\Delta\omega_0\Omega_{ce}}{\Delta\omega_0^2 - \Omega_{ce}^2})[\hat{e}_z.\nabla_\perp \times \delta\hat{E}_\perp + \beta_{0e}\nabla_\perp.\delta\hat{B}_\perp] \quad (7)$$

$$\delta\hat{\rho}_p = \frac{i\omega_b^2\gamma_{0e}}{4\pi\omega^2}(1 + \frac{\omega_T^2}{A\omega^2})k(\hat{e}_z.\delta\hat{E})$$
$$-\frac{i\omega^2}{\omega^2 - (\Omega_{ce}\gamma_{0e})^2}(\nabla_\perp.\delta\hat{E}_\perp)$$
$$-\frac{\omega\Omega_{ce}\gamma_{0e}}{\omega^2 - (\Omega_{ce}\gamma_{0e})^2}(\hat{e}_z.\nabla_\perp \times \delta\hat{E}_\perp) \quad (8)$$

By employing Maxwell's equations and Floquent's theorem, the fluctuating transverse electric and magnetic fields is derived. The results are:

$$\nabla^2\mathbf{E} - \frac{1}{c^2}\frac{\partial^2\mathbf{E}}{\partial t^2} = \frac{\nabla\rho}{\varepsilon_0} + \mu_0\frac{\partial\mathbf{J}}{\partial t} \quad (9)$$

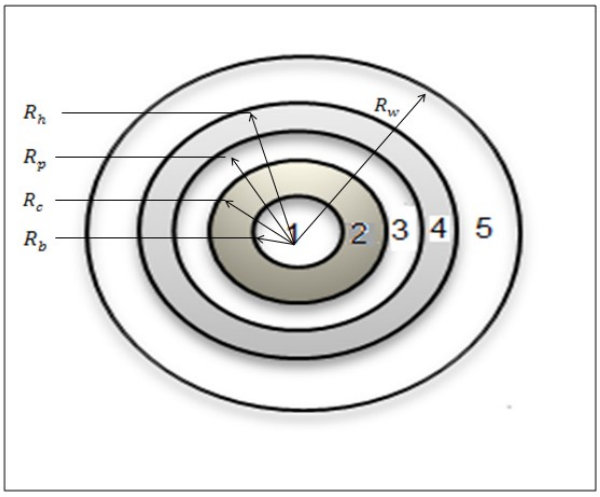

Figure 1. Schematic of the helix TWT structure cross section.

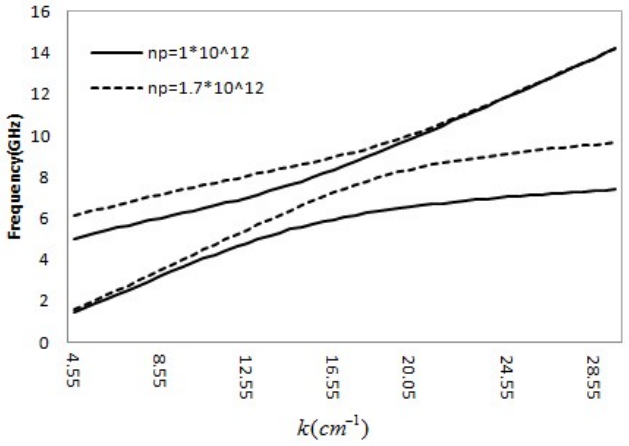

Figure 2. Graph of the frequency versus wavenumber for $n_p = 1\times10^{12}cm^{-3}$, $n_p = 1.7\times10^{12}cm^{-3}$

$$\delta\hat{E}_\perp = \frac{i}{\chi_0^2}[k\nabla_\perp\delta\hat{E}_z - \frac{\omega}{c}\hat{e}_z\times\nabla_\perp\delta\hat{B}_z - \frac{4\pi\omega}{c^2}\delta\hat{J}_\perp] \quad (10)$$

$$\delta\hat{B}_\perp = \frac{i}{\chi_0^2}[k\nabla_\perp\delta\hat{B}_z + \frac{\omega}{c}\hat{e}_z\times\nabla_\perp\delta\hat{E}_z - \frac{4\pi k}{c}\hat{e}_z\times\delta\hat{J}_\perp] \quad (11)$$

in which $\chi_0^2 = \omega^2/c^2 - k^2$.

Using equations 5-8 as well as 10 and 11 simultaneously and with the aid of equation 9, the wave equation will be derived as follows:

Region 2:

$$(\nabla_\perp^2 + \chi_{+,I,bp}^2)(\nabla_\perp^2 + \chi_{-,I,bp}^2)\delta\hat{E}_z = 0 \quad (12)$$

$$(\nabla_\perp^2 + \chi_{+,I,bp}^2)(\nabla_\perp^2 + \chi_{-,I,bp}^2)\delta\hat{B}_z = 0 \quad (13)$$

Region 1 and 3:

$$(\nabla_\perp^2 + \chi_{+,II,p}^2)(\nabla_\perp^2 + \chi_{-,II,p}^2)\delta\hat{E}_z = 0 \quad (14)$$

$$(\nabla_\perp^2 + \chi_{+,II,p}^2)(\nabla_\perp^2 + \chi_{-,II,p}^2)\delta\hat{B}_z = 0 \quad (15)$$

$\chi_{\pm,I,bp}^2$, $\chi_{\pm,II,p}^2$ and the related coefficients are given in [7].

Region 4 and 5:

$$(\nabla_\perp^2 + \chi_0^2)\delta\hat{E}_z = 0 \quad (16)$$

$$(\nabla_\perp^2 + \chi_0^2)\delta\hat{B}_z = 0 \quad (17)$$

The solutions of 12 – 17 can be written as follows:

$$\delta E_z = AJ_l(\chi_{\pm,II,p^r}), \qquad 0 \le r \le R_b$$

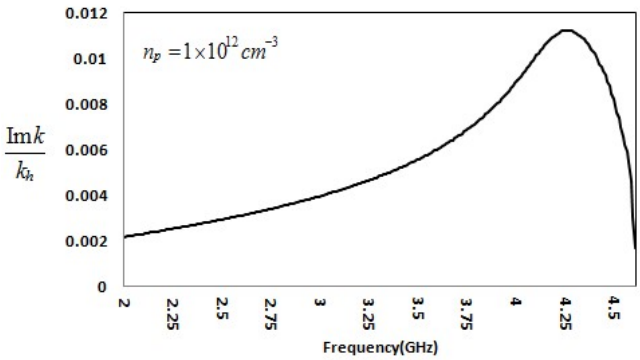

Figure 3. The normalized growth rate versus frequency $n_p = 1\times10^{12}cm^{-3}$, $I_b - 0.4A$.

$$BJ_l(\chi_{\pm,I,bp^r}) + CY_l(\chi_{\pm,I,bp^r}), \qquad R_b < r < R_c$$

$$DJ_l(\chi_{\pm,II,p^r}) + EY_l(\chi_{\pm,II,p^r}), \qquad R_c < r < R_p$$

$$FJ_l(\chi_{0r}) + GY_l(\chi_{0r}), \qquad R_p < r < R_h$$

$$H[J_l(\chi_{0r})\acute{Y}_l(\chi_0 R_w) - \acute{J}_l(\chi_0 R_w)Y_l(\chi_{0r})], \qquad R_h < r \le R_w \quad (18)$$

and

$$\delta B_z = A1J_l(\chi_{\pm,II,p^r}), \qquad 0 \le r \le R_b$$

$$B1J_l(\chi_{\pm,I,bp^r}) + C1Y_l(\chi_{\pm,I,bp^r}), \qquad R_b < r < R_c$$

$$D1J_l(\chi_{\pm,II,p^r}) + E1Y_l(\chi_{\pm,II,p^r}), \qquad R_c < r < R_p$$

$$F1J_l(\chi_{0r}) + G1Y_l(\chi_{0r}), \qquad R_p < r < R_h$$

$$H1[J_l(\chi_{0r})\acute{Y}_l(\chi_0 R_w) - \acute{J}_l(\chi_0 R_w)Y_l(\chi_{0r})], \quad R_h < r \le R_w \quad (19)$$

The dispersion relation is obtained using the appropriate boundary conditions.

$$[\frac{-(M30\zeta21 - M24\zeta24)}{(-\zeta21\zeta23 + \zeta22\zeta24)}]$$

$$[\frac{M19M40\zeta17}{M19} + \frac{M41Z19\zeta20}{Z19}]$$

$$+[\frac{-(-M30\zeta22 + M24\zeta23)}{(-\zeta21\zeta23 + \zeta22\zeta24)}]$$

$$[\frac{M19M49\zeta18}{M19} + \frac{M41Z19\zeta19}{Z19}] = 0 \quad (20)$$

The coefficients were obtained in our previous work in [7].

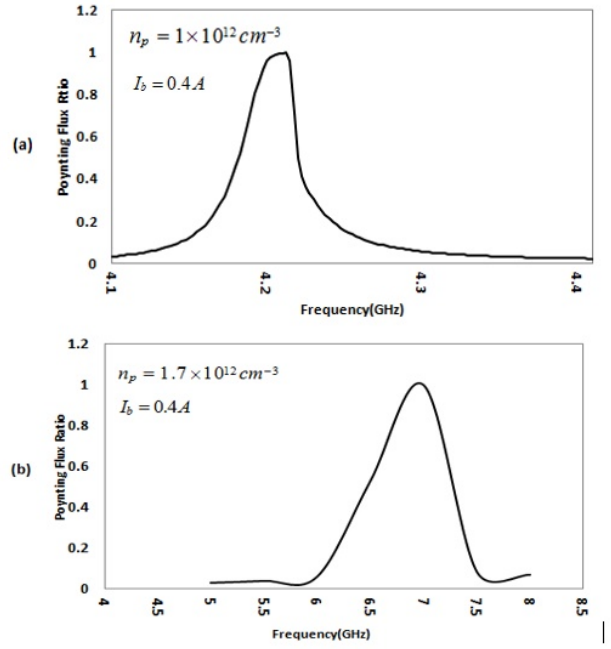

Figure 4. Poynting flux ratio of the plasma region to the total poynting flux for (a)$n_p = 1\times10^{12}\text{cm}^{-3}$, $I_b - 0.4\text{A}$ and (b) $n_p = 1.7\times10^{12}\text{cm}^{-3}$, $I_b = 0.4\text{A}$.

4. Poynting flux

The poynting vector represents the energy transfer per unit area per unit time of an electromagnetic field. The group velocity is the slope of $\omega - k$ curve at any point. The group velocity is also the speed at which energy is propagated along the system. According to our investigation the group velocity is non-zero for the plasma mode representing that there is a real power flow associated with these modes.
The total power flow along the helical sheath is given by the poynting vector:

$$\mathbf{P} = \frac{1}{2} Re \int \delta\mathbf{E} \times \delta\mathbf{H}^* \tag{21}$$

This equation is written as follows in all TWT structure regions:

$$\begin{aligned} P = {} & \pi Re[\int_0^{R_b} (\delta\hat{E}_{1r}\delta\hat{H}^*_{1\theta} - \delta\hat{E}_{1\theta}\delta\hat{H}^*_{1r})rdr \\ & + \int_{R_b}^{R_c} (\delta\hat{E}_{2r}\delta\hat{H}^*_{2\theta} - \delta\hat{E}_{2\theta}\delta\hat{H}^*_{2r})rdr] \\ & + \pi Re[\int_{R_c}^{R_p} (\delta\hat{E}_{3r}\delta\hat{H}^*_{3\theta} - \delta\hat{E}_{3\theta}\delta\hat{H}^*_{3r})rdr \\ & + \int_{R_p}^{R_h} (\delta\hat{E}_{4r}\delta\hat{H}^*_{4\theta} - \delta\hat{E}_{4\theta}\delta\hat{H}^*_{4r})rdr] \\ & + \pi Re[\int_{R_h}^{R_w} (\delta\hat{E}_{5r}\delta\hat{H}^*_{5\theta} - \delta\hat{E}_{5\theta}\delta\hat{H}^*_{5r})rdr] \end{aligned} \tag{22}$$

The fluctuating electric and magnetic fields in different regions of the TWT are given in the appendix A.

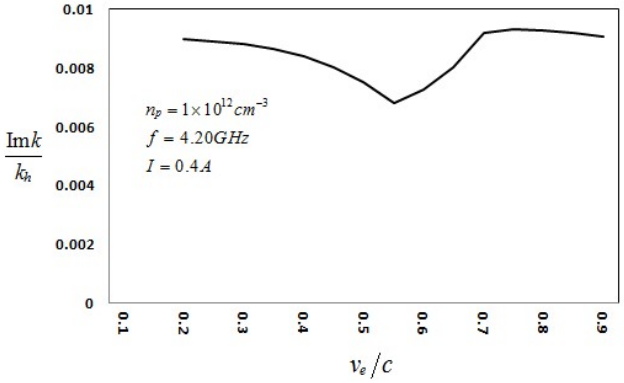

Figure 5. Plot of the growth rate versus beam velocity for the structure of Fig. 1 $n_p = 1\times10^{12}\text{cm}^{-3}$,$f = 4.20\text{GHz}$, $I = 0.4\text{A}$.

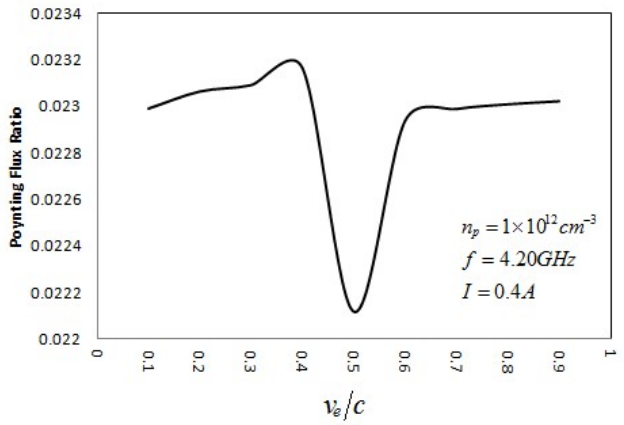

Figure 6. Poynting flux ratio versus beam voltage $n_p = 1\times10^{12}\text{cm}^{-3}$,$f = 4.20\text{GHz}$, $I = 0.4\text{A}$.

5. Numerical results

In this section, we show the effect of thermal plasma on the normalized growth rate $|fracImkk_h$ of a helix type amplifier via the numerical solution of a dispersion Relation **??** [7]. We can fix the principal parameters for the helix as $\lambda_h = 0.1256\text{cm}$, $\delta_h = 0.035$ cm, $R_h = 1.0\text{cm}$, $R_w = 2.5\text{cm}$ and $R_p = 0.5\text{cm}$.
The function $\omega(k)$ is known as the dispersion relation. Dispersion is when the distinct phase velocities of the components of the envelope cause the wave packet to spread out over time. Fig. 2 depicts the dispersion characteristic for thermal plasma of density $n_p = 1\times10^{12}\text{cm}^{-3}$ and $n_p = 1.7\times10^{12}\text{cm}^{-3}$ in the absence of an electron beam. As can be seen from the figure, the lower branch at low wave numbers represents the electromagnetic mode and the upper branch represents the plasma guide mode. But at high wavenumber the lower curve represents the plasma guide mode and the upper branch represents the electromagnetic wave [9]. The two curves converge near the mid-wave numbers. Here is a situation in which the hybrid wave is formed [10–12]. For the particular case reviewed $n_p = 1\times10^{12}\text{cm}^{-3}$, the frequency of the hy-

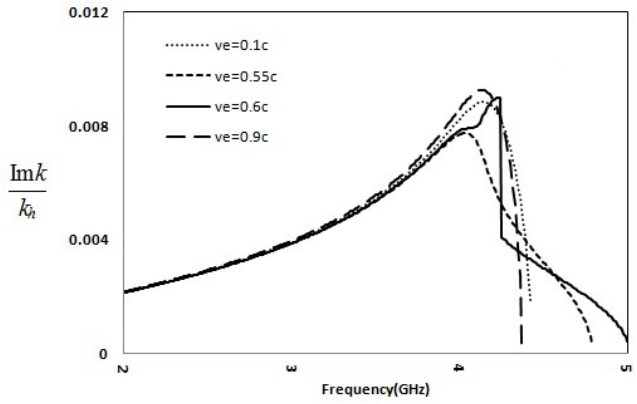

Figure 7. The normalized growth rate versus frequency for several beam voltage $n_p = 1 \times 10^{12}$ cm^{-3}, $I = 0.4$ A.

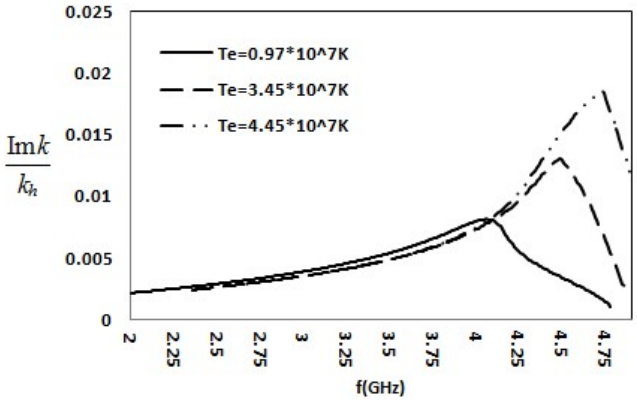

Figure 8. Illustration of the variation of the normalized growth rate versus frequency for different plasma temperature $n_p = 1 \times 10^{12}$ cm^{-3}.

brid wave is $f = 4.20$GHz while this frequency increases for $n_p = 1.7 \times 10^{12}$cm^{-3}[7].

The normalized growth rate of the structure versus frequency is shown in Fig. 3 for an electron beam of current 0.4A.It can be seen from this figure that the maximum growth rate has occurred at a frequency of 4.20GHz, which is where the hybrid mode developed.

Fig. 4(a) and 4(b) reveal the ratio of the axial poynting flux in the region of thermal plasma to the total poynting flux in the five regions, for two different plasma densities. These figures indicate that this ratio represents the amount of power present in the plasma region. Extracting this power from the plasma is important, as the amplified power tends to concentrate in the plasma region.

For $n_p = 1 \times 10^{12}$cm^{-3}, the poynting flux ratio reaches its maximum value at the hybrid mode frequency. Far from this point the interaction is with the electromagnetic wave and the poynting flux is small. This is true for other densities. Here we consider only one density $n_p = 1 \times 10^{12}$cm^{-3}.

A representative plot of the normalized growth rate as a function of the beam velocity is shown in Fig. 5 when the frequency is fixed at the hybrid mode frequency $f = 4.20$GHz for $n_p = 1 \times 10^{12}$cm^{-3}.

As shown in the figure, the normalized growth rate reaches a minimum at $v_b = 0.55c$. The effect of variations of the beam velocity on the poynting flux ratio is displayed in Fig. 6 for a fixed beam current $I = 0.4$A at the hybrid mode frequency of $f = 4.20$GHz.

According to the dispersion curve shown earlier in Fig. 2, the region of the hybrid wave is within the plasma wave number. The interaction of the electron beam with a plasma mode at high and low beam velocities causes concentration of the poynting flux in the plasma region. However, the interaction of the electron beam with the hybrid wave is far more effective. It can be seen that at some medium beam velocities, the beam interacts with a hybrid wave and gives more energy to amplify the wave. Thus, the concentration of the poynting flux in the plasma region is lower, and the maximum growth rate will occur at this beam velocity.

Fig. 7 reveals the normalized growth rate versus the frequency for different beam velocities. As expected, according to our previous results, the frequency of the maximum growth rate is near the frequency of the hybrid mode for all beam velocities. Narrowing curves represent the interaction of the electron beam with the plasma mode while broader curves show the same interaction with the structure mode.

Fig. 8 displays the variation of the normalized growth rate to frequency for different plasma temperature at $v_b = 0.55c$ which is the optimal beam velocity in which the beam interacts with the hybrid wave. As can be seen from the figure the growth rate will increase with increased plasma temperature. The figure shows that we always obtain the maximum normalized growth rate at the frequency of hybrid wave.

6. Conclusion

This was a supplementary article to our previous paper where the interaction of the hollow electron beam by the electromagnetic wave was examined. This paper suggested that the interaction of the electron beam with the hybrid mode was far more effective. Thus, at the hybrid mode frequency, the electron beam would give more energy to the wave and the electromagnetic wave would be amplified further. At points other than this frequency, the electron beam only interacted with electromagnetic waves, so the amount of energy it could transmit was small.

Conflict of interest statement:

The authors declare that they have no conflict of interest.

References

[1] J. R. Pierce and L. M. Field. *Proceedings of the IRE*, **35**:108, 1947.

[2] L. J. Chu and J. D. Jackson. *Proceedings of the IRE*, **36**:853, 1945.

[3] M. Chodorow and N. J. Nalos. *Proceedings of the IRE*, **44**:649, 1956.

[4] O. E. H. Rydbeck. *Ericsson Technics*, **46**:3, 1948.

[5] N. I. Karbushev. *Radiophysics and Quantum Electronics*, **34**:825, 1991.

[6] S. Saviz. *IEEE Trans. Plasma Sci.*, **42**:2023, 2014.

[7] M. Mehranfar, Sh. Saviz, and D. Dorranian. *IEEE Trans. Plasma Sci.*, **47**:12315, 2019.

[8] S. Kobayashi, T. M. Antonsen, and G. S. Nusinovich. *IEEE Trans. Plasma Sci.*, **26**:669, 1998.

[9] CaltechTHESIS problem! -, -:–, -.

[10] F. Shahi and S. Saviz. *IEEE Trans, Plasma Sci.*, **44**:1800, 2016.

[11] L. Pu-Kun and X. Hong-Quan. *Chin. Phy. B*, **16**:766, 2007.

[12] S. Saviz and F. Shahi. *IEEE Trans. Plasma Sci.*, **42**:917, 2014.

Appendix A

As can be seen from the article, in order to calculate the poynting flux, it is necessary to calculate different electric and magnetic fields in different regions. For this purpose, we first started by calculating $\delta J_\perp$ and δJ_z. To derive $\delta J_\perp$ and δJ_z in different region we can use equations 9-12:
Region 2:

$$\delta\hat{J}_{\perp,I} = -\frac{c}{4\pi}\frac{1}{\Lambda_{+bp}\Lambda_{-bp}}([A_b+A_p+A_{bp}]\nabla_\perp\delta\hat{E}_z$$

$$+[B_b+B_p+B_{bp}]\hat{e}_z\times\nabla_\perp\delta\hat{B}_z$$

$$+[D_b+D_p+D_{bp}]\hat{e}_z\times\nabla_\perp\delta\hat{E}_z+[E_b+E_p]\nabla_\perp\delta\hat{B}_z)$$

$$A_b=\frac{\alpha_b\Lambda_{0b}(ck-\omega\beta_{0e})}{\Delta\omega_0},A_p=\frac{\alpha_p\Lambda_{0b}ck}{\omega}$$

$$A_{bp}=-\alpha_b\alpha_p(ck-\omega\beta_{0e})(\frac{1}{\Delta\omega_0}-\frac{\Omega_{ce}^2\gamma_{0e}}{\omega\Delta\omega_0^2})+ck(\frac{1}{\omega}-\frac{\Omega_{ce}^2\gamma_{0e}}{\omega^2\Delta\omega_0})$$

$$B_b=-\alpha_b\Lambda_{0b},B_p=-\alpha_p\Lambda_{0p},B_{bp}=-\alpha_b\alpha_p2(\frac{\Omega_{ce}^2\gamma_{0e}}{\omega\Delta\omega_0}-1)$$

$$D_b=\alpha_b[\frac{i\Omega_{ce}}{\Delta\omega_0^2}(ck-\omega\beta_{0e})],D_p=\alpha_p[\frac{i\Omega_{ce}\gamma_{0e}}{\omega^2}(ck)]$$

$$D_{bp}=-i\alpha_b\alpha_p((ck-\omega\beta_{0e})(\frac{\Omega_{ce}}{\Delta\omega_0^2}-\frac{\Omega_{ce}\gamma_{0e}}{\omega\Delta\omega_0})$$

$$+ck(\frac{\Omega_{ce}\gamma_{0e}}{\omega^2}-\frac{\Omega_{ce}}{\omega\Delta\omega_0}))$$

$$E_b=\alpha_b[\frac{i\Omega_{ce}}{\Delta\omega_0}],E_p=\alpha_p[\frac{i\Omega_{ce}\gamma_{0e}}{\omega}]$$

$$\Lambda_{\pm bp}=1-\frac{\omega_b^2\Delta\omega_0}{c^2\chi_0^2(\Delta\omega_0\mp\Omega_{ce})}-\frac{\omega_p^2\gamma_{0e}\omega}{c^2\chi_0^2(\omega\mp\Omega_{ce}\gamma_{0e})}$$

$$\alpha_b=\frac{\omega_b^2\Delta\omega_0^2}{c^2\chi_0^2(\Delta\omega_0^2-\Omega_{ce}^2)}$$

$$\alpha_p=\frac{\omega_p^2\gamma_{0e}\omega^2}{c^2\chi_0^2(\omega^2-(\Omega_{ce}\gamma_{0e})^2)}$$

$$\Lambda_{0b}=[1-\frac{\omega_b^2}{c^2\chi_0^2}]$$

$$\Lambda_{0p}=[1-\frac{\omega_p^2\gamma_{0e}}{c^2\chi_0^2}]$$

$$\delta\hat{J}_{z,I}=[\frac{i\omega_b^2\omega\gamma_{0e}}{(4\pi\Delta\omega_0^2\gamma_{0e}^2)}+\frac{i\omega_p^2\gamma_{0e}}{(4\pi\omega)}]\delta\hat{E}_z$$
$$+i\omega_b^2\Delta\omega_0^2\beta_{0e}\frac{1}{(4\pi\Delta\omega_0^2(\Delta\omega_0^2-\Omega_{ce}^2)\chi_0^2)}$$
$$+\bar{A}_{eT}\nabla_\perp^2\delta\hat{E}_z+A_{bT}\nabla_\perp^2\delta\,\hat{B}_z$$

$$\bar{A}_{eT}=\bar{A}_{ep}+O_{T1}$$

$$\bar{A}_{bT}=\bar{A}_{bp}+O_{T1}$$

$$\bar{A}_{bp}=(\frac{i\omega}{\Lambda_{+bp}\Lambda_{-bp}})[\frac{\alpha_b\Omega_{ce}}{\Delta\omega_0}+\frac{\alpha_p\Omega_{ce}\gamma_{0e}}{\omega}]$$
$$+(\frac{i\Omega_{ce}\gamma_{0e}}{\Lambda_{+bp}\Lambda_{-bp}})(\alpha_b\Lambda_{0b}+\alpha_p\Lambda_{0p}$$
$$+2\alpha_p\alpha_b(\frac{\Omega_{ce}^2\gamma_{0e}}{\omega\Delta\omega_0}-1))+\Omega_{ce}\gamma_{0e}$$

$$\bar{A}_{ep}=k+(\frac{\omega}{\Lambda_{+bp}\Lambda_{-bp}})(\frac{\alpha_b\Lambda_{0b}(k-\omega\beta_{0e})}{\Delta\omega_0}$$

$$+(\frac{\alpha_p\Lambda_{0p}k}{\omega}-\alpha_p\alpha_b((k-\omega\beta_{0e})(\frac{1}{\Delta\omega_0}-\frac{\Omega_{ce}^2\gamma_{0e}}{\Delta\omega_0^2\omega})+k(\frac{1}{\omega}-\frac{\Omega_{ce}^2\gamma_{0e}}{\Delta\omega_0^2\omega^2}))))$$
$$+(\frac{\Omega_{ce}\gamma_{0e}}{\Lambda_{+bp}\Lambda_{-bp}})[\frac{\alpha_b\Omega_{ce}(k-\omega\beta_{0e})}{\Delta\omega_0^2}+(\frac{\alpha_pk\Omega_{ce}\gamma_{0e}}{\omega^2}-\alpha_p\alpha_b(k-\omega\beta_{0e})\times(\frac{\Omega_{ce}}{\Delta\omega_0^2}-\frac{\Omega_{ce}\gamma_{0e}}{\omega\Delta\omega_0})+k(\frac{\Omega_{ce}\gamma_{0e}}{\omega^2}-\frac{\Omega_{ce}}{\omega\Delta\omega_0}))]$$

$$O_{T1}=-\frac{\omega_p^2\gamma_{0e}\chi_0^{-2}\omega_T^2(1-\frac{\omega_T^2}{\omega^2})^{-1}}{\omega^2-(\Omega_{ce}\gamma_{0e})^2}-\frac{\omega_p^2\gamma_{0e}\omega\omega_T^2}{\chi_0^2(k\omega^2-(\Omega_{ce}\gamma_{0e})^2)(1-\frac{\omega_T^2}{\omega^2})\Lambda_{+bp}\Lambda_{-bp}}$$
$$[\frac{\alpha_b\Lambda_{0b}(k-\omega\beta_{0e})}{\Delta\omega_0}+(\frac{\alpha_p\Lambda_{0p}k}{\omega}-\alpha_p\alpha_b((k-\omega\beta_{0e})(\frac{1}{\Delta\omega_0}-\frac{\Omega_{ce}^2\gamma_{0e}}{\Delta\omega_0^2\omega})+k(\frac{1}{\omega}-\frac{\Omega_{ce}^2\gamma_{0e}}{\Delta\omega_0^2\omega^2})))]$$
$$-\frac{\omega_p^2\gamma_{0e}^2\Omega_{ce}\omega_T^2}{\chi_0^2(\omega^2-(\Omega_{ce}\gamma_{0e})^2)k(1-\frac{\omega_T^2}{\omega^2})\Lambda_{+bp}\Lambda_{-bp}}\frac{\alpha_b\Omega_{ce}(k-\omega\beta_{0e})}{\Delta\omega_0^2}+\frac{\alpha_p\Omega_{ce}\gamma_{0e}k}{\omega^2}$$
$$-\alpha_p\alpha_b(k-\omega\beta_{0e})(\frac{\Omega_{ce}}{\Delta\omega_0^2}-\frac{\Omega_{ce}\gamma_{0e}}{\omega\Delta\omega_0})+k(\frac{\Omega_{ce}\gamma_{0e}}{\omega^2}-\frac{\Omega_{ce}}{\omega\Delta\omega_0})$$

$$O_{T2}=-\frac{i\omega_p^2\gamma_{0e}^2\chi_0^{-2}\Omega_{ce}\omega_T^2(1-\frac{\omega_T^2}{\omega^2})^{-1}}{k(\omega^2-(\Omega_{ce}\gamma_{0e})^2)}-\frac{i\omega_p^2\gamma_{0e}\omega\omega_T^2}{\chi_0^2(k\omega^2-(\Omega_{ce}\gamma_{0e})^2)(1-\frac{\omega_T^2}{\omega^2})\Lambda_{+bp}\Lambda_{-bp}}\frac{\alpha_b\Omega_{ce}}{\Delta\omega_0}$$
$$+\frac{\alpha_p\Omega_{ce}\gamma_{0e}}{\omega}-\frac{i\omega_p^2\gamma_{0e}^2\Omega_{ce}\omega_T^2}{\chi_0^2(\omega^2-(\Omega_{ce}\gamma_{0e})^2)k(1-\frac{\omega_T^2}{\omega^2})\Lambda_{+bp}\Lambda_{-bp}}$$
$$\times[\alpha_b\Lambda_{0b}+\alpha_p\Lambda_{0p}+2\alpha_p\alpha_b(\frac{\Omega_{ce}^2\gamma_{0e}}{\omega\Delta\omega_0}-1)]$$

Regions 1 and 3:

$$\delta\hat{J}_{\perp,II}=-\frac{c}{4\pi}R_p\frac{ck}{\omega}\nabla_\perp\delta\hat{E}_z-\hat{e}_z\times\nabla_\perp\delta\hat{B}_z+i[\frac{ck}{\omega}\hat{e}_z\times\nabla_\perp\delta\hat{E}_z+\nabla_\perp\delta\hat{B}_z]$$

$$\delta\hat{J}_{z,II}=\frac{i\omega_p^2\gamma_{0e}}{4\pi\omega}[1+\frac{\omega_T^2}{A\omega^2}]\delta\hat{E}_z+[(\frac{\omega_p^2\gamma_{0e}}{4\pi\omega})(\frac{\omega_T^2}{A\omega k})(\frac{\omega}{\omega^2-(\Omega_{ce}\gamma_{0e})^2})(\frac{1}{r}+\frac{\partial}{\partial r})]\delta\hat{E}_r$$
$$+[(\frac{\omega_p^2\gamma_{0e}}{4\pi\omega})(\frac{i\omega_T^2\Omega_{ce}\gamma_{0e}}{A\omega k(\omega^2-(\Omega_{ce}\gamma_{0e})^2)})\times(-\frac{1}{r}-\frac{\partial}{\partial r})]\delta\hat{E}_\theta$$

In turn, the fluctuating electric and magnetic fields are:
Region 2:

$$\delta\hat{E}_r=\frac{i}{\chi_0^2}[k\frac{\partial\delta\hat{E}_z}{\partial r}+\frac{\omega}{c}\frac{1}{\Lambda_{+bp}\Lambda_{-bp}}[A_b+A_p+A_{bp}]\frac{\partial\delta\hat{E}_z}{\partial r}+[E_b+E_p]\frac{\partial\delta\hat{B}_z}{\partial r}]$$

$$\delta\hat{B}_r=\frac{i}{\chi_0^2}[k\frac{\partial\delta\hat{B}_z}{\partial r}+(\frac{k}{\Lambda_{+bp}\Lambda_{-bp}})-[B_b+B_p+B_{bp}]\frac{\partial\delta\hat{B}_z}{\partial r}-[D_b+D_p+D_{bp}]\frac{\partial\delta\hat{E}_z}{\partial r}]$$

$$\delta\hat{E}_\theta=\frac{i}{\chi_0^2}[(\frac{\omega}{c})\frac{\partial\delta\hat{E}_z}{\partial r}+(\frac{k}{\Lambda_{+bp}\Lambda_{-bp}})[A_b+A_p+A_{bp}]\frac{\partial\delta\hat{E}_z}{\partial r}+[E_b+E_p]\frac{\partial\delta\hat{E}_z}{\partial r}]$$

Regions 1 and 3:

$$\delta\hat{E}_r=\frac{i}{\chi_0^2}[k\frac{\partial\delta\hat{E}_z}{\partial r}+\frac{\omega}{c}R_P(\omega,k)(\frac{\partial}{\partial r})[\frac{ck}{\omega}\delta\hat{E}_z+i\delta\hat{B}_z]]$$

$$\delta\hat{B}_r=\frac{i}{\chi_0^2}[k\frac{\partial\delta\hat{B}_z}{\partial r}-ikR_P(\omega,k)(\frac{\partial}{\partial r})[\frac{ck}{\omega}\delta\hat{E}_z+i\delta\hat{B}_z]]$$

$$\delta\hat{B}_\theta=\frac{i}{\chi_0^2}[\frac{\omega}{c}\frac{\partial\delta\hat{E}_z}{\partial r}+kR_P(\omega,k)(\frac{\partial}{\partial r})[\frac{ck}{\omega}\delta\hat{E}_z+i\delta\hat{B}_z]]$$